ELSEVIER

Journal of Alloys and Compounds 446–447 (2007) 72–79

Journal of ALLOYS AND COMPOUNDS

www.elsevier.com/locate/jallcom

LiAl-substitution into the MgH_2 structure may improve the hydrogen storage processes

Jian-jie Liang

Accelrys Inc., 10188 Telesis Ct., San Diego, CA 92121, USA

Received 23 October 2006; received in revised form 3 December 2006; accepted 4 December 2006
Available online 25 January 2007

Abstract

When Li,Al is coupled-substituted into the MgH_2 structure to assume the composition of $LiAlMg_{10}H_{24}$, the resulted structure was found to retain that of the parent material but assumes substantial differences in bonding and associated properties. Density functional theory (DFT) method was used in deriving the stable structure, computing the thermochemical parameters and evaluating the reaction/activation energies of dehydriding. The stability of the optimized LiAl-substituted structure was verified through the lattice dynamics calculations of the density functional perturbation theory (DFPT) method. The coupled substitution weakens the H-metal bonds that results in reductions in the reaction energy and potentially the activation barriers of dehydriding of the materials.

Keywords: MgH_2; LiAl-substitution; Hydrogen storage; DFT; Reaction energy/barrier of dehydriding

1. Introduction

Difficulty in finding efficient, inexpensive hydrogen storage materials is one of the major obstacles in realizing the new hydrogen economy worldwide. The problem is particularly acute with respect to vehicle onboard hydrogen storage [1]. There had been considerations of various types, and one category of materials had been the MgH_2 structure that offers a theoretical H-storage capacity of 7.6 wt% of the type material, MgH_2. Recent discovery [2] of chemical activation of MgH_2 revived the interest in using the MgH_2 type materials for vehicle onboard applications of hydrogen storage. It opened up the door for exploring a whole series of materials of similar nature.

Theoretical modeling of the density functional theory (DFT) method had been successfully applied to studies of relative phase stabilities [3] and structure predictions [4] of various (potential) hydrogen storage materials. Such studies on the one hand suggested general directions in tailoring the solid-state substitutions in improving the hydriding/dehydriding processes of the storage materials, and on the other hand revealed fundamental aspects such as chemical bonding characters and temperature/pressure-induced phase transitions of the materials.

In the present work, coupled LiAl-substitution of Mg into the MgH_2 structure to form ordered $LiAlMg_{10}H_{24}$ structure was examined computationally in regard to equilibrium structure, structural stability, thermochemistry and dehydriding properties.

2. Computational details

Density functional theory [5] method of two different implementations, CASTEP [6] and DMol^3 [7], respectively, was utilized (see Section 4.1 for reasons of using multiple implementations and sets of program parameters). CASTEP was primarily used in bulk studies such as unit-cell optimizations and structural stability. Ultrasoft potentials were used where, for H, Li, Mg and Al, valence electrons included $1s^1$, $1s^2\ 2s^1$, $2p^6\ 3s^2$, $3s^2\ 3p^1$, respectively. The plane wave basis set cutoff was 310 eV. The k-point grid was kept to maintain a spacing of ca. 0.05 1/Å. The GGA functional of PW91 [8] was used. The convergence criteria for total energy, max force, max stress, max displacement and SCF iterations were 0.2E−04 eV/atom, 0.5E−01 eV/Å, 0.1 GPa, 0.002 Å and 0.2E−05 eV/atom, respectively. In structural stability and thermochemical studies, CASTEP's implementation of the density functional perturbation theory (DFPT) [9] method was used. Norm-conserving pseudopotentials [10] were used in these calculations. Valence electrons considered were identical to

E-mail address: jjl@accelrys.com.

0925-8388/$ – see front matter © 2006 Elsevier B.V. All rights reserved.
doi:10.1016/j.jallcom.2006.12.027

those as above, except for the Mg species ($3s^2$). The plane wave basis set cutoff was 600 eV. The k-point grid and the DFT functional were again the same as above. The convergence criteria for SCF iterations and phonon convergence (the variation in the electronic second order energy in the linear response scheme in the DFPT calculations [9]) tolerance were 0.1E−07 eV/atom and 0.1E−04 eV/A^2, respectively; DMol^3 was primarily used in calculations regarding dehydriding where surface slabs need to be examined that involved significant portions of vacuum spaces. Program settings and procedures in handling surfaces were identical to those previously reported [11]. The orbital cutoffs for the two new atom species previously not considered, Li and Al, were chosen to be 5.5 and 4.0 Å, respectively. The generalized synchronous transit method [12] was used in the transition state searches.

A supercell (Fig. 1) of $1 \times 2 \times 3$ of the MgH_2 unit cell was constructed as a starting model for the LiAl-substituted structure. Two Mg-atoms in the supercell were replaced by the LiAl pair, and the structure optimized (Fig. 1), followed by a phonon density of state (DOS) calculation in CASTEP.

Complete Linear Synchronous Transit (LST)/Quadratic Synchronous Transit (QST) scheme [12] was used in the transition state searches of the dehydriding processes, complemented by transition state optimization. A surface of the LiAl-substituted materials equivalent to the 1 1 0 surface of the original MgH_2 structure was constructed, with the surface slab extending two unit cell-depth to ensure sufficient bulk

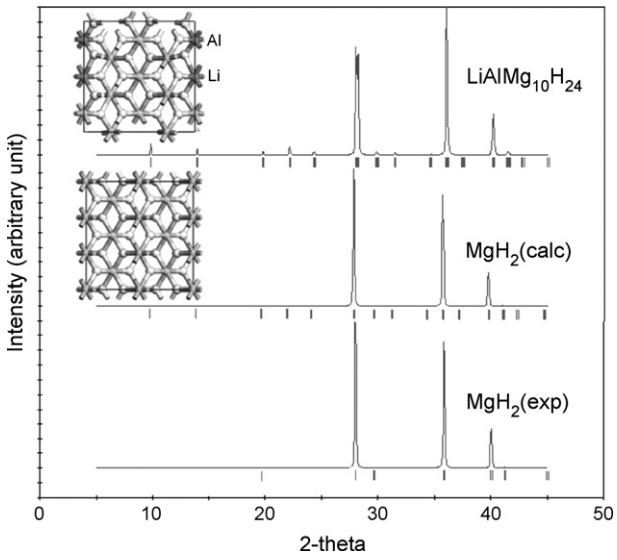

Fig. 1. Simulated powder X-ray diffraction patterns of the structures considered. Instrumental parameters such as profile shape and broadenings had been kept consistent for all structures to ensure comparability. A supercell of $1 \times 2 \times 3$ of the MgH_2 structure is shown to aid the comparison with the unit cell of $LiAlMg_{10}H_{24}$. Atoms not labeled in the structure models: grey: Mg atoms; off-white: H atoms.

Table 1
Crystallographic parameters of structures considered

	MgH_2 (exp.)[a]	MgH_2 (calc.)	$LiAlMg_{10}H_{24}$
Cell content	Mg_2H_4	Mg_2H_4	$LiAlMg_{10}H_{24}$
Theoretical H-capacity (wt%)	7.6	7.6	8.0
Space group	$P4_2/mnm$ (136)	$P4_2/mnm$ (136)	$P2$ (3)
Unit cell dimensions			
a	4.5025 (0.0005)	4.5349	8.9885
b	4.5025 (0.0005)	4.5349	8.9848
c	3.0123 (0.0005)	3.0219	4.4846
α	90	90	90
β	90	90	89.655
γ	90	90	90
Bond length (Å)			
Mg–H	1.95 (0.02), (1.94–1.95)	1.96 (1.96–1.96)	1.95 (1.88–2.06)
Al–H			1.74 (1.70–1.77)
Li–H			2.01 (1.91–2.16)
Zero point vibration energy (ZPE) (kJ/mol_{H2})			
		38.3	38.8
H-metal bond energy (kJ/mol)[b]			
MgMgMg		373.3	370.0 (364.4–372.5)
LiMgMg			353.1 (347.6–358.6)
AlMgMg			356.6 (352.0–361.2)

For average values, their ranges are given immediately underneath corresponding values.
[a] Ref. [25].
[b] Potential energy difference with/without a vacancy in place of an H atom. MgMgMg: H is bonded to 3 Mg-atoms; LiMgMg: H is bonded to one Li and two Mg atoms, respectively; AlMgMg: H is bonded to 1 Al and 2 Mg atoms, respectively.

representation. Parallel calculations were conducted on the unsubstituted MgH_2 system, based on surface slabs of orientation and dimensions comparable to those in the LiAl-substituted system.

3. Results

3.1. Equilibrium structure

Cell dimensions and other crystal chemical parameters of the computed structures were given in Tables 1 and 1a. For the unsubstituted MgH_2 structure, the cell dimensions agree well with those observed experimentally to within 0.3% error range. Geometry optimization of the LiAl-substituted structure resulted in a final structure of space group *P*2. Despite a dramatic lowering of the space group symmetry from tetragonal $P4_2/mnm$ to monoclinic *P*2, the crystal lattice of the new structure is actually pseudo-tetragonal, with *a* and *b* differ by less than 0.004 Å and β close to 90° (by a difference of <0.4°), and bears strong resemblance to the parent structure. The resemblance is most evident in the simulated powder X-ray diffraction (XRD) patterns of the substituted and the parent structures, respectively (Fig. 1), particularly at the dominant diffraction features (peaks near 28, 36, 40° 2θ, respectively). Therefore, there could be a non-trivial likelihood that the LiAl-substituted MgH_2 structure might have already been produced in a lab but undetected.

3.2. Structural stability

An important question to ask on a geometry-optimized structure is whether it will be structurally stable (note this is not the same as thermodynamically stable, which requires additional phase studies). One way for such determination is through the lattice dynamics study of the phonon DOS of the structure [9]. The phonon DOS calculations were done using a k-spacing of ca. 0.05 1/Å for the phonon DOS q-vectors. The results on both the unsubstituted and LiAl-substituted structures revealed no state associated with imaginary frequencies (Fig. 2). The results on the one hand confirmed both the experimental [13] and theoretical [14] studies of the stability of the MgH_2 structure, and on the other hand revealed that the geometry-optimized structure of the LiAl-substituted MgH_2 is structurally stable. Table 1 gives the zero point vibrational energies (ZPE) of the materials derived from the above phonon DOS calculations. The ZPE of 38.3 kJ/mol_{H2} for the unsubstituted MgH_2 structure agrees well with that of the previous study of 38.5 kJ/mol_{H2} using the supercell method [11]. The ZPE of the LiAl-substituted structure differs only slightly from the unsubstituted, with a value of 38.8 kJ/mol_{H2}.

3.3. Chemical bonding

In accordance to the crystallographic resemblance, the unsubstituted and LiAl-substituted structures show similar electron density distributions, which can be quantified through the Mulliken charge distribution analysis (Table 2). In both structures, the H atoms are negatively charged and there is little overlap population between H and Mg. Such charge distribution strongly suggests ionic bonding, that's confirmed by the deformation density distribution (Fig. 3a and b) that corresponds to the total density with the density of the isolated atoms subtracted. The deformation densities are all spherical, and all centered around the H atoms, signature of net charge transfer onto the H atoms (but see discussion bellow regarding H–Al bonding). A similar chemical bonding studies [15] on various MgH_2 struc-

Table 1a
Fractional atomic coordinates of phases in the main table (Table 1)

	x	*y*	*z*
MgH_2 (exp.)			
Mg1	0	0	0
Mg2	0.5	0.5	0.5
H1	0.304	0.304	0
H2	0.696	0.696	0
H3	0.196	0.804	0.5
H4	0.804	0.196	0.5
MgH_2 (calc.)			
Mg1	0	0	0
Mg2	0.5	0.5	0.5
H1	0.305	0.305	0
H2	0.695	0.695	0
H3	0.195	0.805	0.5
H4	0.805	0.195	0.5
$LiAlMg_{10}H_{24}$			
Mg1	0.251	1.001	0.003
Mg2	0.243	0.337	0.000
Mg3	0.246	0.666	0.006
Mg4	0.749	1.001	0.997
Mg5	0.757	0.337	1.000
Mg6	0.754	0.666	0.994
Mg7	0.5	0.168	0.5
Mg8	0.5	0.501	0.5
Mg9	0.5	0.834	0.5
Mg10	0	0.172	0.5
Li	0	0.497	0.5
Al	0	0.832	0.5
H1	0.402	0.999	0.307
H2	0.401	0.333	0.302
H3	0.401	0.671	0.305
H4	0.909	0.980	0.316
H5	0.901	0.329	0.303
H6	0.908	0.697	0.312
H7	0.654	0.165	0.195
H8	0.653	0.504	0.198
H9	0.656	0.834	0.186
H10	0.149	0.159	0.195
H11	0.149	0.506	0.195
H12	0.141	0.838	0.223
H13	0.598	0.999	0.693
H14	0.599	0.333	0.698
H15	0.599	0.671	0.695
H16	0.091	0.980	0.684
H17	0.099	0.329	0.697
H18	0.092	0.697	0.688
H19	0.346	0.165	0.805
H20	0.347	0.504	0.802
H21	0.344	0.834	0.814
H22	0.851	0.159	0.805
H23	0.851	0.506	0.805
H24	0.859	0.838	0.777

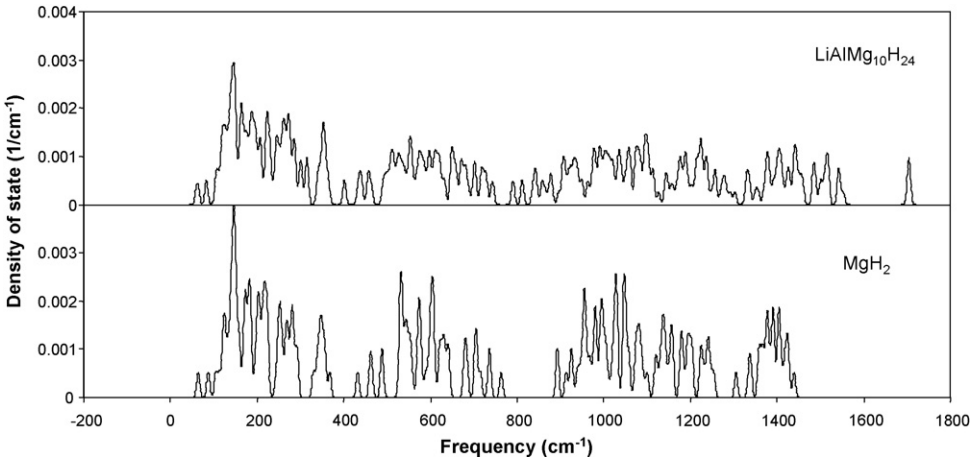

Fig. 2. Phonon DOS of MgH_2 and $LiAlMg_{10}H_{24}$.

ture polymorphs indicated similar Mulliken charge distribution (although there are some differences in the absolute values that can be a function of basis set choices and of the methodology implementation details, which had already been well known [16]). The finding of the same reference of net electron transfer through electron localization function (ELF) study was also confirmed in the deformation electron density study in the present study.

The LiAl-substituted structure nevertheless possesses heterogeneity enough to distinguish itself. Unlike Mg, Al in the structure assumes a low charge and a high positive value in the overlap population, indicating covalent component in bonding [16]. Such covalent component is confirmed by the total electron density distribution (Fig. 3c), where there exists substantial, directional electron density along the H–Al bonds. Note that, however, although there's some overlap population between H and Li (Table 2), the H–Li bonding remains largely ionic (Fig. 3d). Such heterogeneity is directly responsible to the marked changes in structural and physical chemical properties of the material: First, the H-metal bond distances assume broader ranges (Table 1); second, the bond strength of the H atoms to their neighboring species becomes weakened. Table 1 towards the end listed the potential energy difference with/without a vacancy in place of an H atom, which constitutes a reasonable, collective measure of relative bond strength of the H atom to its surrounding atoms. It is evident that (a) the bond strength is different with different bonding environments; (b) bond strength becomes generally lower, even when the H atom is surrounded by three Mg atoms similar to that in the unsubstituted structure.

Table 2
Mulliken charges and overlap populations of the unsubstituted and LiAl-substituted MgH_2 structures, based on the CASTEP calculations

	Mulliken charges		Overlap population
$Mg_{12}H_{24}$			
Mg	1.20	H–Mg	−0.04 (−0.01 to −0.10)
H	−0.60	H–H	−0.06 (−0.04 to −0.12)
$LiAlMg_{10}H_{24}$			
Li	0.65	H–Li	0.21 (0.06–0.28)
Al	0.45	H–Al	0.73 (0.70–0.74)
Mg	1.26 (1.21–1.32)	H–Mg	−0.07 (0.00 to −0.16)
H	−0.57 (−0.50–−0.62)	H–H	−0.06 (−0.01 to −0.16)

The ranges of the values (if exist) are given in brackets.

3.4. Reaction energies and energy barriers of dehydrinding

The hope of the LiAl-substitution is to lower the reaction and activation energies during the dehydriding processes. While a comprehensive evaluation on the impact of the LiAl-substitution on such energies is beyond the reach of the present work, or that of quantum mechanical computations in general (see Section 4), it was chosen here to examine the dehydriding processes on a representative surface, the 1 1 0 surface of the MgH_2 structure [11] and its equivalent in the LiAl-substituted structure, hoping to gain insight into the potential impact of the substitutions. Furthermore, preliminary work showed that there can be multiple dehydriding paths, even on the 1 1 0 surface alone. Therefore, it was chosen here to look at one of the simplest dehydriding paths associated with the 1 1 0 surface, the one-step, direct dehydriding path, to gain preliminary understanding on the potential improvement in the thermodynamic processes in hydriding/dehydrinding of the materials.

The 1 1 0 surface of the MgH_2 structure had been identified [11] to be one of the most prominent faces that have the lowest surface energy. For the unsubstituted structure, initial dehydriding of the surface hydrogen atoms in the neighboring bridge positions (the starting state) on the 1 1 0 surface (refer to the equivalents in the LiAl-substituted structure as in Fig. 4*R* and *R*′) was examined against the ending state with the two hydrogen atoms removed from the surface to form one free hydrogen molecule (refer to the equivalents in the LiAl-substituted structure as in Fig. 4*P* and *P*′). The LST/QST transition state search/optimization based on the above starting and ending configurations yielded a one-step dissociation, with an activation energy of 271.7 kJ/mol_{H2} (the difference in total energies between the configuration before dehydriding and that at the transition state, respectively). The reaction energy, i.e., the total energy difference between the starting and the ending configurations, respectively, was found to be 237.4 kJ/mol_{H2}.

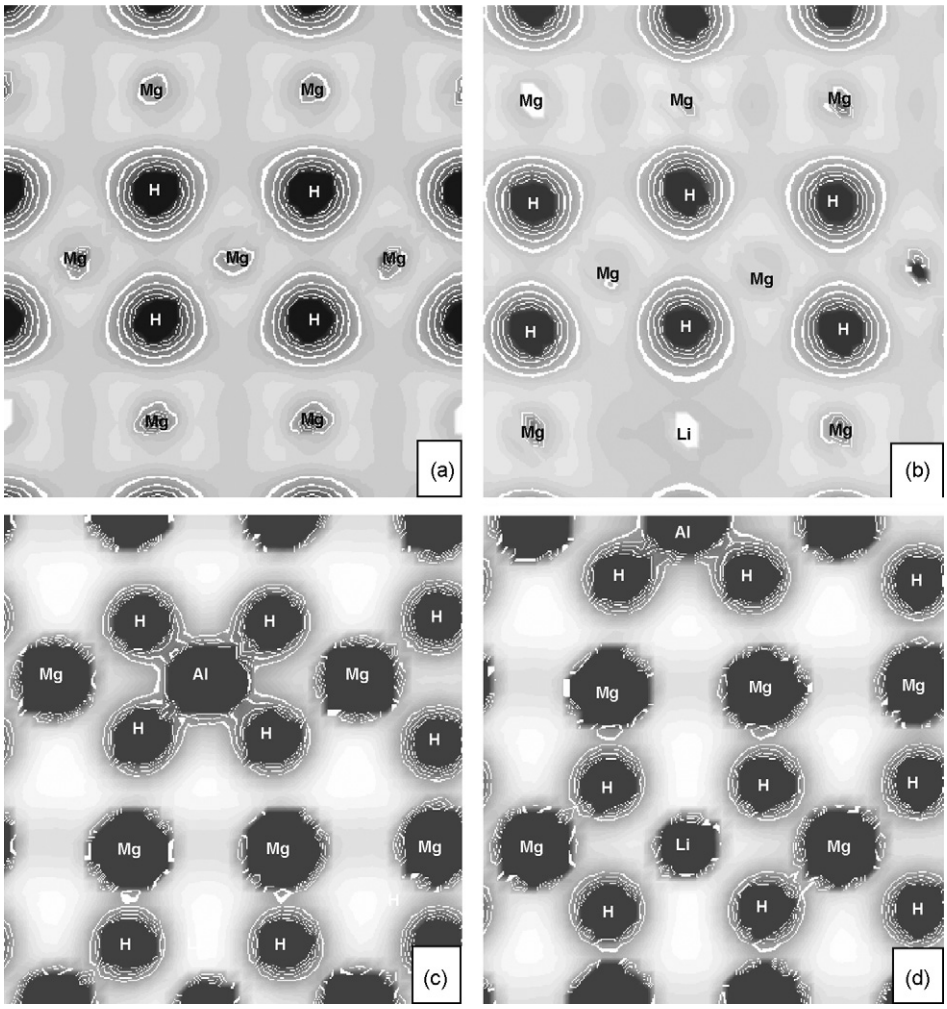

Fig. 3. Electron density distributions of the MgH_2 structure and its LiAl-substituted structure. The dark areas concentrate the electron densities. (a and b) Deformation densities of the unsubstituted and LiAl-substituted MgH_2 structures, respectively. Cross-sections parallel to the 1 1 0 surface (the MgH_2 structure) or that equivalent to the MgH_2 1 1 0 surface (the $LiAlMg_{10}H_{24}$ structure). The contour lines are from 0 to 0.2 in intervals of 0.05 e/Å^3; (c and d) total densities of the LiAl-substituted MgH_2 structure. Cross-sections dissect the Al/Li-H6 bipyramids. The contour lines are from 0.285 to 0.565 in intervals of 0.07 e/Å^3.

On an equivalent surface of the LiAl-substituted structure where the Mg atom is replaced by Al (Fig. 4*R* and *R*′), after the initial LST/QST transition state search, the transition state optimization yielded an intermediate state (the state in Fig. 4*I* and *I*′, corresponding to a local energy well in the reaction path). Two separate transition state searches were subsequently conducted, one between the starting state and the intermediate state, and the other between the intermediate state and the ending state. The results indicated an overall reaction energy of 179.5 kJ/mol$_{H2}$ (157.3 + 22.2), a 34% reduction from that of the unsubstituted (of 237.4 kJ/mol$_{H2}$). It should also be noted that, over the same simple dehydriding path as in the unsubstituted structure in the above, there are now two transition states (Fig. 4*TS1* and Fig. 4*TS2*) associated with this particular dehydriding path, with corresponding activation energies of 187.8 and 36.2 kJ/mol, respectively. The larger of the two activation energies corresponds to the rate-limiting barrier in the whole reaction path. In other words, in the same dehydriding path, the effective activation barrier in the LiAl-substituted structure is reduced from 271.7 to 187.8 kJ/mol, amounting to a reduction of 31%.

4. Discussion

4.1. The use of multiple implementations of the DFT method and sets of program settings

It will be ideal that all DFT calculations are carried out through a single implementation and with an identical set of program settings so that (energy) results will be easily portable and can be compared to each other. However, in real DFT applications, one is constrained by both the necessary approximation of the exchange-correlation functional and the computational tractability of a given application. As a result, many different implementations [17] became available, carrying with them characteristic basis sets, pseudopotentials and, to a lesser extent, unique set of exchange-correlation functionals. Each such implementation offers a unique aspect in real applications, such as that the plan-wave based implementations make it easy in calculating forces and stress, or that the local basis set-based methods allow linear scaling of performance as a function of the number of atoms. The key to determine which implementa-

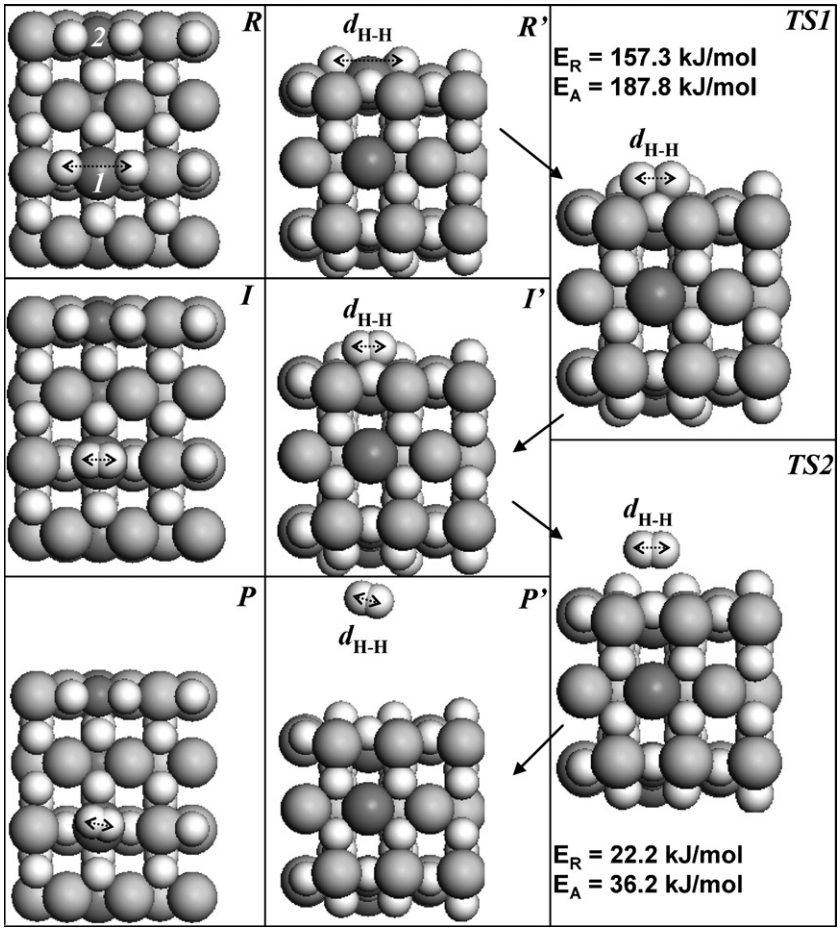

Fig. 4. Dehydriding of the LiAl-substituted MgH_2 structure on a configuration equivalent to the direct (one-step) dehydriding on the 1 1 0 surface of the unsubstituted MgH_2 structure. *R*: Reactant/surface view of MgH_2 1 1 0-equivalent. $d_{H–H} = 3.09$ Å; *I*: Intermediate/surface view when forming the intermediate. $d_{H–H} = 0.84$ Å; *P*: product/surface view after forming H_2 molecule. $d_{H–H} = 0.75$ Å; *R*′, *I*′, *P*′ cross-sectional views of their respective surface counterparts; *TS1*: transition state from *R* to *I* (cross-sectional view). $d_{H–H} = 1.32$ Å; *TS2*: transition state from *I* to *P* (cross-sectional view). $d_{H–H} = 0.82$ Å. Large, grey sphere: Mg; Large, dark-grey sphere: Li (labeled "*1*" in *R*); small, dark-grey sphere: Al (labeled "*2*" in *R*); small, off-white spheres: H. E_R, energy of reaction; E_A, energy barrier.

tion and what parameter set to use lies really in the theoretical abstraction, or "translation" [17], of the real application problem.

In the present work, three self-contained areas were identified: (a) to find the equilibrium geometry of the LiAl-substituted structure based on that of the parent MgH_2 material (Sections 3.1 and 3.3); (b) to determine the structural stability of a given structure (Section 3.2) and (c) to calculate relative energy changes on a surface during a dehydriding process (Section 3.4). Areas *a* and *b* involve calculating forces acting on individual atoms and stresses on the unit cell that are most efficiently dealt with in plane-wave based implementations [17]. Therefore CASTEP, being one of the plan-wave implantations, was chosen. The use of norm-conserving potentials in the DFPT calculations in area *b*, as opposed to using the ultrasoft potentials as used in geometry optimizations in area *a*, was because of that validations had been done using such potentials in the DFPT implementation, just like that the geometry-optimizations had been done in using the ultrasoft potentials; in area *c*, surface studies involve large proportions of vacuum spaces, which means dense plan-waves to account for such spaces if plan-wave based implementation (CASTEP) is used, and in turn wasted computing cycles. On the contrary, DMol^3, being one of the local basis set based implementations, is insensitive to the occurrence of such vacuum spaces, and therefore is much more efficient in the type of calculations.

It 's important to point out that, in each of the above three areas, the respective combinations of DFT implementation/program settings had been independently validated within the individual applications/areas (see earlier discussions of results in each separate areas). Furthermore, within each individual application area, all energy comparisons had been confined to within the area itself, and conclusions were drawn without reaching out (to other areas).

4.2. Possibility of disorder

It should be emphasized here that the configuration derived in the present work is only one of the many configurations possible given the composition/superstructure combination. Preliminary work showed that other configurations (of the same composition) may be structurally stable, as well. This brings up the possibility of random distribution of the Li,Al species in the superstructure that results in a statistically averaged pseudo-symmetry identical to that of the parent materials. Such possibility is, however,

beyond the reach of the current computational approaches, and should most appropriately be proven experimentally.

4.3. Reaction energies and activation barriers

There had been reports [18–21] of a range of apparent activation energies of dehydriding of the pure MgH_2 materials, between 119 and 323 kJ/mol. Given that all sample materials were indeed pure and pre-activated, it's still important to note that all measurements were conducted on bulk materials which can involve different (related or unrelated) processes such as (bulk/surface) diffusions and dehydriding over different crystallographic orientations and surface morphologies, each with its own associated characteristic activation barrier. Therefore, the apparent energy barrier of a given measurement corresponds to an average of barriers effective in the measurement temperature range, only. Furthermore, each of the reports cited a measurement temperature range different from the other, with a given measurement potentially not being able to sample barriers active at higher temperatures that the measurement temperature range did not reach. On the other hand, quantum mechanics-based calculations typically focus on a given surface orientation and assume ideal surface configurations. The results are therefore far from capturing the full picture of the reaction barriers of the materials in the bulk. One should therefore be very careful in making quantitative comparisons between the calculated barriers with those of the experimentally observed. In the present work, only one (the 1 1 0 surface) of the many possible surfaces of the materials was considered, with an ideal surface configuration. In addition, the dehydriding processes of the LiAl-substituted structure were examined while focusing only around the Al atom in the structure. Therefore, the results so obtained can in no way be sufficient to be used quantitatively to represent the whole material(s). It nevertheless does not prevent the qualitative conclusions, or the *trends*, being drawn on system improvements with regard to the thermodynamic properties upon the chemical substitutions.

4.4. Thermochemical considerations

It should be noted that, while proving structural stability, phonon DOS calculations does not address the issue of thermodynamic stability of the postulated compound of $LiAlMg_{10}H_{24}$. The issue itself calls for comprehensive evaluations and is beyond the scope of the present work. Yet, some preliminary thermochemical consideration regarding possible reaction pathways for the target compound will still be helpful. One may consider the following two potential (solid-state) reactions:

$$LiAlH_4 + 10MgH_2 \rightarrow LiAlMg10H_{24} \quad (R1)$$

$$LiH + AlH_3 + 10MgH_2 \rightarrow LiAlMg_{10}H_{24} \quad (R2)$$

Based on the known crystal structures of the reactants, LiAlH4 [22], LiH [23], AlH3 [24] and MgH2 [25], the binding energies (with ZPE corrections) of the reactants were calculated to be −1334.0, −246.7, −1535.7 and −699.8 kJ/mol, respectively, with that of the postulated phase being −6710.2 kJ/mol. The reaction enthalpies for the above two reactions can then subsequently calculated to be, respectively,

$$\Delta H_{R1} = 135.1\,\mathrm{kJ/mol_{H2}}$$

$$\Delta H_{R1} = 172.5\,\mathrm{kJ/mol_{H2}}$$

The reaction enthalpies for both reactions are significantly endothermic. One will have to hope and rely on the differences in heat capacity and entropy of the reactant materials to turn the reaction free energy to be exothermic as a function of temperature. More likely than not, one may eventually have to use an unconventional approaches, such as mechanical alloying through high-energy ball-milling, to synthesize the postulated compound.

5. Conclusion

The DFT calculations revealed that there exists a structurally stable crystalline phase of the nominal composition, $LiAlMg_{10}H_{24}$, of the MgH_2 structure type. There exist indications that the coupled LiAl-substitution of the Mg atoms into the structure enables substantial lowering of the total reaction energy and the energy barriers in the dehydriding processes.

Acknowledgements

I thank the HP Company for providing the computing resources. Comments on the draft of the manuscript from my colleagues, Alexander Goldberg, Paul W-C Kung, Max Peterson and George Fitzgerald are greatly appreciated.

References

[1] L. Schlapbach, A. Zuttel, Nature 414 (2001) 353.
[2] S.R. Johnson, P.A. Anderson, P.P. Edwards, I. Gameson, J.W. Prendergast, M. Al-Mamouri, D. Book, I.R. Harris, J.D. Speight, A. Walton, Chem. Commun. 22 (2005) 2823.
[3] M.E. Arroyo y de Dompablo, G. Ceder, J. Alloys Compd. 364 (2004) 6.
[4] P. Vajeeston, P. Ravindran, A. Kjekshus, H. Fjellvåg, Alloys Compd. 404–406 (2005) 377.
[5] P. Hohenberg, W. Kohn, Phys. Rev. B 136 (1964) 864.
[6] M.D. Segall, P.J.D. Lindan, M.J. Probert, C.J. Pickard, P.J. Hasnip, S.J. Clark, M.C. Payne, J. Phys.: Condens. Matter. 14 (2002) 2717.
[7] B. Delley, J. Chem. Phys. 92 (1990) 508.
[8] J.P. Perdew, Y. Wang, Phys. Rev. B45 (1992) 13244.
[9] S. Baroni, S. de Gironcoli, A. dal Corso, P. Giannozzi, Rev. Mod. Phys. 73 (2001) 515.
[10] M.H. Lee, PhD Thesis, Cambridge University, 1996.
[11] J.-J. Liang, Appl. Phys. A 80 (2005) 173.
[12] N. Govind, M. Petersen, G. Fitzgerald, D. King-Smith, J. Andzelm, Comp. Mater. Sci. 28 (2003) 250–258.
[13] J.R. Santisteban, G.J. Cuello, J. Dawidowski, A. Fainstein, H.A. Peretti, A. Ivanov, F.J. Bermejo, Phys. Rev. B 62 (2000) 37.
[14] H.G. Schimmel, M.R. Johnson, G.J. Kearley, A.J. Ramirez-Cuesta, J. Huot, F.M. Mulder, Mater. Sci. Eng. B108 (2004) 38.
[15] P. Vajeeston, P. Ravindran, B.C. Hauback, H. Fjellvåg, A. Kjekshus, S. Furuseth, M. Hanfland, Phy. Rev. B 73 (2006) 224102.
[16] M.D. Segall, R. Shah, C.J. Pickard, M.C. Payne, Phys. Rev. B 54 (1996) 16317–16320.
[17] J. Hafner, C. Wolverton, G. Ceder, MRS Bull. 31 (2006) 659.
[18] J.F. Fernandez, C.R. Sanchez, J. Alloys Compd. 340 (2002) 189.

[19] C. Stander, J. Inorg. Nucl. Chem. 39 (1977) 221.
[20] T.R. Jensen, A. Andreasen, T. Vegge, J.W. Andreasen, K. Ståhl, A.S. Pedersen, M.M. Nielsen, A.M. Molenbroek, F. Besenbacher, Int. J. Hydrogen Energy 31 (2006) 2052.
[21] N. Hanada, T. Ichikawa, H. Fujii, J. Phys. Chem. B 109 (2005) 7188–7194.
[22] H.W. Brinks, B.C. Hauback, J. Alloys Compd. 354 (2003) 143.
[23] Y. Fukai, The Metal-Hydrogen System, in: Springer Series in Material Science, vol. 21, Springer-Verlag, Berlin, 1993.
[24] J.W. Turley, H.W. Rinn, Inorg. Chem. 8 (1969) 18.
[25] B.H. Zachariasen, C.E. Holley Jr., J.F. Stamper Jr., Acta Cryst. 16 (1963) 352.